ELSEVIER

Signal Processing 46 (1995) 233–242

SIGNAL PROCESSING

Detection of occluded circular objects by morphological operators

A. Ray Chaudhuri[a], B. Chanda[b], B.B. Chaudhuri[a,*]

[a]*Computer Vision & Pattern Recognition Unit, Indian Statistical Institute, 203 B.T. Road, Calcutta 700035, India*
[b]*Electronics and Communication Sciences Unit, Indian Statistical Institute, Calcutta, India*

Received 23 June 1994; revised 17 November 1994, 28 February 1995, 2 March 1995 and 31 May 1995

Abstract

In this article we propose a simple and fast method to locate circular objects from binary images even if they are highly occluded by one another. The algorithm is based on basic morphological transforms and thus can be implemented on parallel machines. Some examples are presented to illustrate the efficiency of the approach.

Zusammenfassung

In diesem Artikel stellen wir eine einfache und schnelle Methode vor, um runde Objekte in binären Bildern zu erkennen, sogar wenn sie sich stark überdecken. Der Algorithmus basiert auf morphologischen Transformationen und kann deshalb auf parallelen Maschinen implementiert werden. Beispiele präsentieren und illustrieren die Effizienz der gewählten Methode.

Résumé

Dans cet article, nous proposons une méthode simple et rapide, pour la detection d'objets circulaires dans des images binaires, quandmême s'ils sont hautement fermés l'un par l'autre. L'algorithm est basé sur des transformations morphologiques fondamentales, et peut ainsi être utilisé sur des machines parallèles. Quelques exemples sont présentés pour illustrer l'efficacité de cette méthode.

Keywords: Circular object detection; Occlusion; Mathematical morphology

1. Introduction

Identifying circular objects and estimating their parameters are of great importance in various applied fields. If a vision system is put to operate in a real environment to recognize, count, pick up and place different size of disk-type objects, it is expected to work reliably and fast. In reality, for large number of disks, some may be highly occluded by one another and it is often necessary to detect them and estimate their parameters under such situation (Fig. 1).

* Corresponding author. E-mail: bbc@isical.ernet.in.

SSDI 0165-1684(95)00085-2

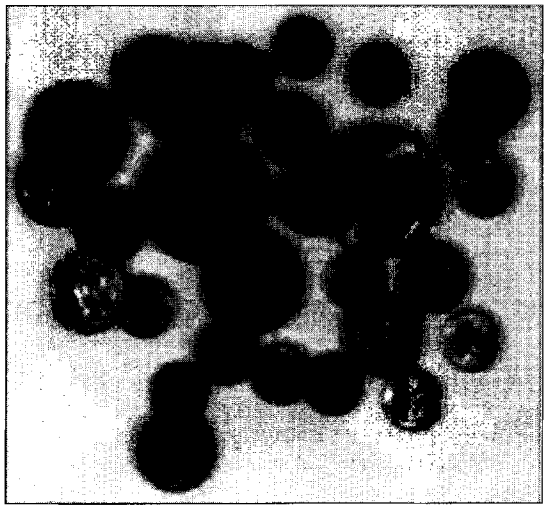

Fig. 1. A front-lit image of some coins.

Circular objects can be detected by methods like Hough transform or by basic geometric and heuristic approaches [2–4, 6, 8–10]. Circular shapes can also be detected using mathematical morphology (MM) although we have not come across any paper on morphology dealing solely with this problem. The present work is an attempt to fill up this gap. It has been shown that the proposed method can separate circular objects even if they are highly occluded.

MM operators are suitable for parallel implementation of algorithm. Though they are usually slow on serial machines, some fast algorithms for dilation and erosion [5] can speed up the entire process considerably.

In Section 2 we have presented some basic definitions of MM operations. The approach used to detect circular objects is described in Section 3 where the problem of noise is also treated by using morphological operators. Some experimental results and discussion are presented in Section 4. The algorithm for separating occluded disks is given in Appendix A.

2. Basic definitions

In MM there are two basic operations: dilation and erosion. Other operators are derived from these two operations. However, dilation and erosion can be constructed from even lower level set-operations like translation, set-union and set-intersections [7, 12]. Let A and B be subsets of $\mathscr{Z}^2$ and let t be a point (pixel) in $\mathscr{Z}^2$. In our application, A and B denote sets of points (pixels) in digital space. Here we treat A as *object* and B as *structuring element* by which A is morphologically operated.

1. The *translation* of A by t, denoted by A_t and the reflection of A, denoted by $\tilde{A}$ are defined, respectively, as

$$A_t = \{p \in \mathscr{Z}^2 \mid p = a + t; a \in A\};$$

$$\tilde{A} = \{-p \mid p \in A\}.$$

2. The *dilation* and *erosion* of A by B, denoted by $A \oplus B$, and $A \ominus B$, respectively, are defined as

$$A \oplus B = \{p \in \mathscr{Z}^2 \mid p = a + b; a \in A \text{ and } b \in B\};$$

$$A \ominus B = \{p \in \mathscr{Z}^2 \mid (p + b) \in A; \forall b \in B\},$$

The *conditional dilation* of A by B within a set $I \in \mathscr{Z}^2$, denoted by $A \oplus |_I B$, is defined as

$$A \oplus |_I B = (A \oplus B) \cap I.$$

3. The *opening* and *closing* of A by B, denoted by $A \circ B$ and $A \bullet B$, respectively, are defined as

$$A \circ B = (A \ominus B) \oplus B; \qquad A \bullet B = (A \oplus B) \ominus B.$$

4. The *morphological pattern spectrum* or simply *image spectrum* $S_i(A, \mathscr{K})$ of an object A with respect to a set of structuring elements $\mathscr{K} = \{K_1, K_2, K_3, \ldots)$ can be defined as

$$S_i(A, \mathscr{K}) = \#(A \circ K_i) \quad \text{for } i = 1, 2, 3, \ldots,$$

where $\#X$ denotes the area of the object X, which in our case, is the number of pixels in X.

5. A set transformation $\Psi(\bullet)$ is said to be a *morphological filter* if for any two sets X and Y in the domain of the transformation,

(i) $X \subset Y \Rightarrow \Psi(X) \subset \Psi(y)$ (increasing),

(ii) $\Psi[\Psi(X)] = \Psi(X)$ (idempotence).

6. Discrete circle: A *discrete circle* with radius r and center (α, β) is a set $T_{[r]}(\alpha, \beta)$ of 8-connected

pixels so that each pixel (x, y) satisfying the inequality

$$0 \leqslant |\sqrt{(x-\alpha)^2 + (y-\beta)^2}| < r + 1/2.$$

The 8-connected inner border of the disk denoted by $C_{[r]}(\alpha, \beta)$, is defined by the pixels (x, y) satisfying the inequality

$$r - 1/2 < |\sqrt{(x-\alpha)^2 + (y-\beta)^2}| < r + 1/2.$$

If the center is at origin $(0,0)$ we simply use $T_{[r]}$ and $C_{[r]}$.

3. Method and implementation

Let E_0 be the union of given disks D_{ij} with radius r_i and center c_j; $(i,j) \in \mathscr{I} \subset \mathscr{Z}^2$. Henceforth it will be assumed that r_i's are strictly monotonically increasing, i.e. $1 < r_1 < r_2 < r_3 \cdots < r_N$ and $c_0 = (0,0)$. At binary level a disk is occluded if it has a non-empty intersection with another disk. We assume that no disk is completely occluded (i.e. intersection of the border of any disk with the border of E_0 is not null). We try to quantify the level of occlusion of a disk in the following manner.

Level of occlusion of a disk. A disk D_{ij} is said to be a *Level2 occluded* disk (or simply L_2 disk) in E_0 if its center c_j is contained in another disk D_{lk}, where $r_l > r_i$. Otherwise, an occluded disk is said to be a *Level1 occluded* disk (or simply L_1 disk). If not occluded at all, then a disk is called a *Level0* (L_0) disk.

The proposed method is based on the following three observations in analog domain that can be verified easily.

(i) A disk remains unchanged if it is opened by another structuring disk having smaller or equal radius

$$D_{ij} \circ D_{lk} = D_{ij}, \quad r_i \geqslant r_l. \tag{1}$$

(ii) Union of circular disks with radii greater than the radius of the structuring disk will remain unchanged due to opening

$$\left(\bigcup_{i,j} D_{ij}\right) \circ D_{lk} = \bigcup_{i,j} D_{ij} \quad \forall r_i \geqslant r_l \text{ and } \forall c_j. \tag{2}$$

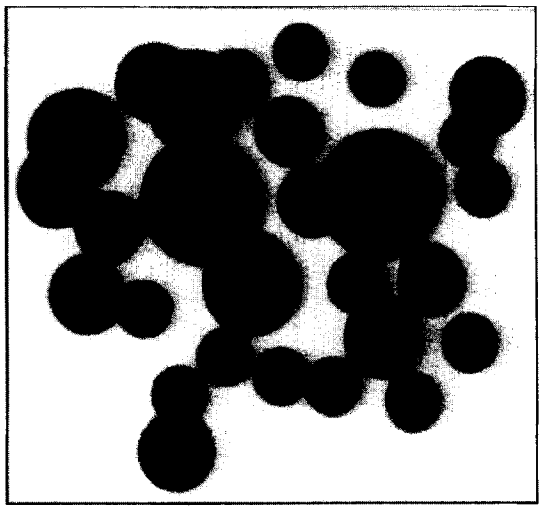

Fig. 2. The back-lit image of that same.

(iii) If there exists an L_1 disk D_{ij} in E_0 then eroding E_0 by the structuring disk D_{i0} will result in an isolated point at the center c_j and other components. Consider an L_2 disk D_{ij} so that its center c_j can be included in a disk D_{lk} $(r_l > r_i)$. If E_0 is eroded by the same structuring disk D_{i0} then no isolated point at c_j results. However, c_j is included in the connected component of the eroded version of $D_{lk} \cup D_{ij}$.

The present algorithm is devised to work with binary images. In our experimental set-up, we used back-lighting condition to obtain the images. In the back-lighting condition, the source is situated at the back of the objects and acing the camera. The back-lit image (Fig. 2) can be segmented to binary image by a threshold t, where t is the average of the minimum gray value $f_{\min}$ and maximum gray value $f_{\max}$ of the image. We found uniformly good results for all back-lit test images by using the procedure.

The proposed algorithm is based on basic morphological transforms described above. It consists of two basic steps namely (a) estimating the radii of possible existing circular objects, and (b) separation of disks in the image.

3.1. Estimation of the radii

We can estimate the radii of possible existing circular objects in two ways – supervised and

unsupervised. In the unsupervised case there is no a priori knowledge of possible radii of the disks in a scene while in a supervised case a set of possible circular objects are available. Their radii are estimated using morphological operators.

3.1.1. Unsupervised method

In this case we estimate the existing radii by taking pattern spectrum (PS) of the input binary image E_0 (from which we have to locate and separate the existing disks). The PS of E_0 is nothing but a stepwise recursive opening process with discrete structuring disk $T_{[r+n\times k]}$, where k is the step size (usually $k = 1$); the initial value r is less than the minimum possible disk's radius. However, the camera should be calibrated in such a way that the radius always becomes more than 10 pixels because circularity of a discrete disk is established reasonably well when its radius exceeds 10 [1]. The opening continues until the cardinality, i.e. the number of object pixels of $E_0 \circ T_{[r+n\times k]}$ becomes zero. The PS of E_0 is represented by a histogram of cardinality versus the radius (see Fig. 3 which is PS graph of Fig. 2). In the histogram each step-jump preceded by a considerable flat step in the histogram will correspond approximately to an existing disk radius. This technique works well if occlusion level is not too high, viz., all disks are of utmost L_1 type.

3.1.2. Supervised method

Here we first take an image of all supplied disks of different sizes that could appear in a scene. The image is such that all disks are distinct and well separated. The radii can be estimated using pattern spectrum method discussed above. However, if the disks are arranged in increasing size so that in the image the connected component corresponding to kth disk is larger than the component corresponding to $(k-1)$th disk then an efficient serial approach is as follows.

Each component is eroded iteratively with the inner boundary of the discrete circle with increasing radius. For example, the kth component, say E_k is eroded with $C_{[r]}$ iteratively where the iteration starts with $r = r_{k-1}$ which is the estimated radius of $(k-1)$th component and r is incremented by 1 until $E_k \ominus C_{[r]} = \phi$.

Note that in supervised radius estimation method, the exact radii of all different sized disks are detected. But in real images there is a possibility that one disk-type object (say with radius r_i) rests on another disk of certain thickness and gets tilted. The resulting image of the disk becomes elliptic in shape, making the maximal disk contained in that elliptic portion smaller than r_i. So, at the disk separating stage, the estimated radii may be slightly less than the actual values.

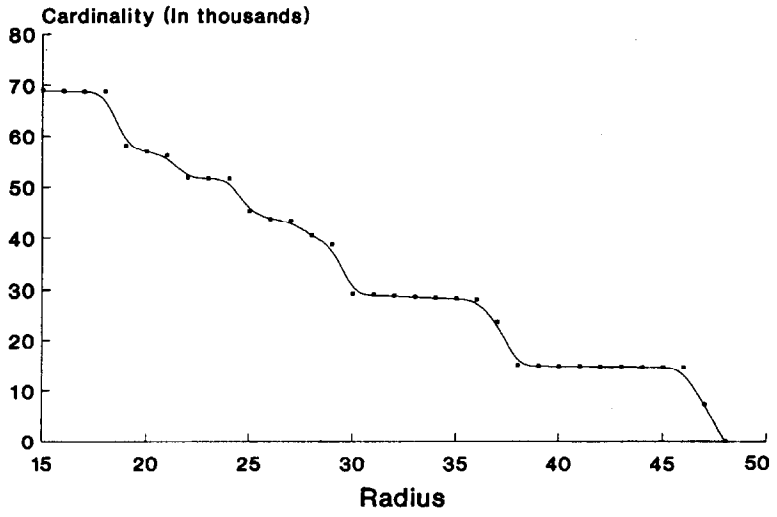

Fig. 3. The graph of the pattern spectrum of the image shown in Fig. 2.

3.2. Separation of the disks

After estimating $r_1, r_2, \ldots, r_N$ of all possible existing disks we perform identification, location and separation step by step within a loop of the algorithm. The execution of the loop once can separate all disks of a particular radius. We describe how this is done in a loop for a particular radius say, r_i.

Step 1: Erode the original image, E_o by the structuring disk $T_{[r_i]}$; let it be E^e.
Open E_o by $T_{[r_{(i+1)}]}$. Suppose it be denoted by $E^{o(+1)}$.

Step 2: Subtract $E^{o(+1)}$ from E^e and let the result be denoted by E^{sc}. If $\#(E^{sc}) = 0$ (i.e. $E^{sc} = \phi$) then there is neither L_0 nor L_1 disk of radius r_i in E_o. Otherwise, E^{sc} is the collection of pseudocentres of L_0 and L_1 disks of radius r_i where pseudocentre of a disk is a very small region containing the actual center of the disk. If existing disks in E_o are perfectly circular then any pseudocentre represents the center of an L_0 or L_1 disk. Otherwise, a pseudocentre represents a small region whose mean position will represent the center. So, from pseudocentres, all the L_0 and L_1 disks of radius r_i can be separated. After separating all L_0 and L_1 disks we check the existence of L_2 disk in the following way.

Step 3: From the opening of the original image E_o by the structuring disk $T_{[r_i]}$, the union of $E^{o(+1)}$ and all separated L_0 and L_1 disks of radius r_i are subtracted (i.e. set difference). Let the difference be denoted by E^{cre}. If the area of E^{cre} is more than a threshold then L_2 disk(s) may exist in the image. In our experiments the value of the threshold is taken as the one-third area of disk of radius r_i. Actually, E^{cre} consists of crescent-like structures, but all of them may not correspond L_2 disk(s) of radius r_i. For example, if a larger disk is opened by a smaller one, its edge will be depleted due to discreteness in the digital domain and some very thin crescent-like structures may appear which do not correspond to any L_2 disk. For further screening a minimum thickness criterion has been considered.

Step 4: E^{cre} will be eroded by a structuring disk. The radius of the structuring disk, r_i which is derived by minimum thickness criteria as follows:

$$r_i' = \frac{(\sqrt{2}-1)r_i}{2\sqrt{2}} \approx 0.146 r_i. \tag{3}$$

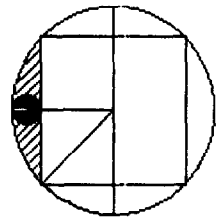

Fig. 4. An illustration of the thickness criteria of a disk.

See Fig. 4 in which the radius of the small darker disk represents the minimum thickness value. $\#(E^{cre} \ominus T_{[r_i']}) > 0$ confirms the existence of L_2 disk(s) in the image. Moreover, each component, say e_j in that eroded part of E^{cre} represents an L_2 disk of radius r_i. Let the region of e_j be grown as a single component in E^{cre} and stored as E^a.

Step 5: To locate the center of that disk, we first locate a small region within which the center should lie. Let the maximum m-times iterative erosion by unit disk of the component e_j is non-null. This iteratively eroded part, $e_j \ominus mT_{[1]}$ is conditionally dilated by $T_{[r_i - r_i' - m + 1]}$ with respect to $E^{o(+1)}$. Let that region be denoted by E^{cfr}. This E^{cfr} contains the center of the L_2 disk.

Step 6: For finding the center, an optimal curve and area fitting technique is used as follows. Find the inner border of E^a; let it be E^b.

For all points $p(x,y) \in E^{cfr}$, compute $\alpha_p = \#(E^a \cap T_{[r_i]}(x,y))$; and $\beta_p = \#(E^b \cap C_{[r_i]}(x,y))$; Select a point $c \in E^{cfr}$ as the center of the disk if

$$((\alpha_c \geqslant \alpha_p) \wedge (\beta_c \geqslant \beta_p)) \text{ is TRUE} \quad \forall p \in E^{cfr}. \tag{4}$$

Thus from all the crescents having a considerable thickness, L_2 disks can be detected. Some major steps in L_1 and L_2 disks separation are shown in Figs. 5 and 6.

Fig. 5(1) shows the original image E_o where the objects appear as light gray. Fig. 5(2) shows E^e (the result of eroding E_o by $T_{[r_i]}$ i.e. output of step 1) in light gray superposed on E_o (in dark gray). Fig. 5(3) is obtained by subtracting $E^{o(+1)}$ from E^e which has been denoted by E^{sc} (output of step 2) and is shown in light gray. Fig. 5(4) shows the detected L_1 disk in light gray, superposed on E_o.

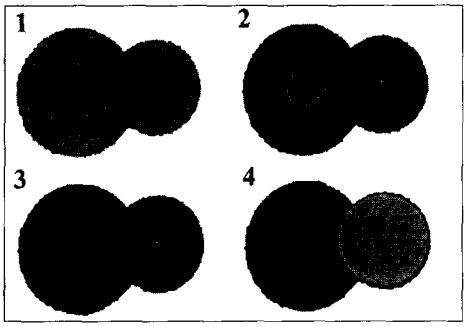

Fig. 5. The major steps in L_1 disk separation are illustrated.

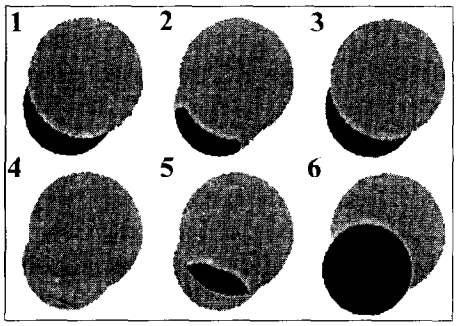

Fig. 6. The major steps in L_2 disk separation are illustrated.

Fig. 6(1) shows E^{cre}, the crescent shape of an L_2 disk in dark gray and is superposed on the original E_o in light gray (output of step 3). e_j (intermediate result of noise cleaning of the crescent E^{cre} in step 4) is shown in dark gray in Fig. 6(2). The dark gray region of Fig. 6(3) is the componentwise growing of e_j in E^{cre} (output of step 4). Fig. 6(4) is the result of recursive m-times erosion of e_j by unit disk (intermediate result of step 5). Fig. 6(5) is the output of step 5 where the m-times erosion of e_j is conditionally dilated by $T_{[r_i - r'_i - m + 1]}$ in $E^{o(+1)}$. The detected L_2 disk in dark gray is shown in Fig. 6(6).

We implemented the algorithm in such a way that the original image is opened only once for each structuring disk of given radius. Because $(E_o \circ T_{[r_i]})$ is used to find disks of radius r_{i-1} and r_i, $E_o \ominus T_{[r_i]}$ and $(E_o \ominus T_{[r_i]}) \oplus T_{[r_i]}$ are computed while locating disks of radius r_{i-1} and the computed results are retained until the location of disks of radius r_i is completed.

The algorithm for separation of disks is presented in Appendix A.

3.3. Removal of noise

The proposed morphological circular shape detector can work well if the image is at least free from foreground noise. But the original binary image may be degraded by both foreground (salt) and back-ground (pepper) noise. As our algorithm is robust under background noise and sensitive under foreground noise, the salt noise removal is essential and preferable before the suppression of background noise. Closing is a good morphological filter for eliminating foreground noise but (especially in presence of background noise) some blurring may take place at the concave corners of the object which causes mislocation and even incorrect identification (especially in case of L_2 disks). More involved techniques are *alternating filters* and *alternating sequential filters*. The alternating filters is constructed by a composition of opening and closing and the alternating sequential filter is constructed by an alternating series of increasing size morphological openings and closings [11]. Since opening enhances the foreground noise, direct use of such filters are not effective.

What we need here is some method which can remove noise and also preserves concave corners. For a moderately noisy image, almost all noise pixels are isolated or *nearly isolated*. By a nearly isolated pixel, we mean a pixel whose all 4-connected horizontal and vertical neighbors or 8-connected diagonal neighbors are of opposite color to that of the pixel. Note that nearly isolated noise pixels include isolated noise pixels (e.g. foreground isolated noise pixels have all eight neighbors belonging to the object). Our algorithm starts with removing these pixels.

Let E be a degraded binary image under additive noise [13]. Let

$$g(E) = E \cup (E \ominus B_1) \cup (E \ominus B_2);$$

$$h(E) = E \cup (E \ominus B_3); \qquad i(E) = E^c;$$

$$\mathcal{N}_*(E) = \#(*(E)/E);$$

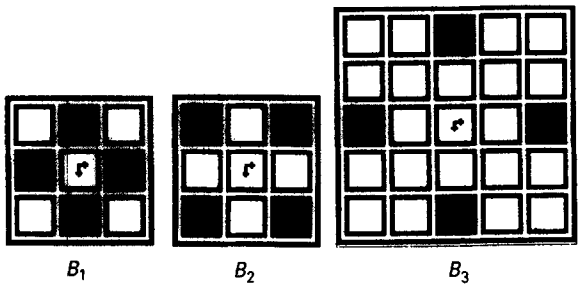

Fig. 7. Structuring elements (B_1, B_2, B_3) for the noise removal.

where $*$ is either g or h and B_1, B_2 and B_3 are illustrated in Fig. 7(a)–(c).

We have removed noise by combining transforms g, h and i in a sequential way. The quantity $\mathcal{N}_{(*)}(\bullet)$ has been used to control the sequential process.

At first note that $g(E)$ is free from nearly isolated salt noise. All nearly isolated 0-pixels whose horizontal and vertical 4-connected neighbors are 1 and all nearly isolated 0-pixels whose 8-connected diagonal neighbors are 1, are converted to 1-pixels by B_1 and B_2, respectively. Note that $\mathcal{N}_g(E)$ is the number of almost isolated 0-pixel of E that has been removed by g. If $\mathcal{N}_g(E) = 0$, then it is assumed that E is free from foreground noise. So no further processing for foreground noise removal is done. If $\mathcal{N}_g(E) > 0$ then $g(g(E)) = g^2(E)$ is computed. $g^2(E)$ cleans salt noise blobs of size somewhat bigger than nearly isolated pixels (e.g. 'L'-like structure of 4-connected three pixels). Now, iff $\mathcal{N}_g(g(E)) > 0$, we compute $h(g^2(E))$. It can be verified that $hg^2(E)$ is free from foreground connected noise components which can maximally contain 2×2 blobs.

The background noise can also be removed in a similar manner as follows. At first take the complement of the transformed foreground noise free image (say, E') and then compute $g(i(E'))$. If $\mathcal{N}_g(i(E')) > 0$ then compute $g^2i(E')$. Again, as in foreground case iff $\mathcal{N}_g(gi(E')) > 0$, compute $hg^2i(E')$.

The composite transform ihg^2ihg^2 has been extensively used over several images and quite satisfactory results are obtained (see, for example Fig. 11).

For images with high degree of noise, the border of the disk gets degraded. Also, blobs of size 3×3 and above can be generated within the disk. A composite transform like $ig^2hg^2ig^2hg^2$ can remove noise blobs of size 3×3, but cannot repair the border deformation. In such a situation $ihg^2ihg^2(E)$ is morphologically closed by a small structuring disk (default radius is 2) and then opened by the same structuring disk. Note that the composite transform of closing followed by an opening is an alternating morphological filter [11].

4. Results and conclusion

The method proposed in the previous section is tested on several synthetic disk images as well as several back-lit images of circular coins of different size. The back-lit images were thresholded to form binary images. Some results for real disks are shown in Figs. 8 and 9. It is noted that disks can be identified at various levels of occlusion. However, here the centers are sometimes slightly displaced and the estimated radii are often smaller than the true ones. This is due to tilting of the disk partially sitting on another disk of certain thickness as explained at the end of Section 3.1.2. Another reason is the under estimation of radius from pattern spectrum. Slight under estimation can take care of the disk boundary noise.

The algorithm is robust in the presence of background noise. We observed that the disks are

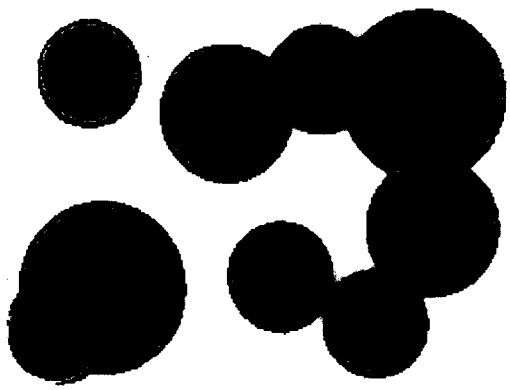

Fig. 8. A binary image of coins and the output with different levels of occlusion.

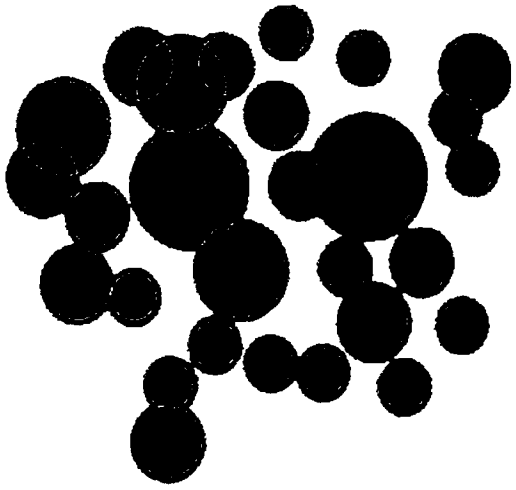

Fig. 9. The binary version of the image in Fig. 2 with its output.

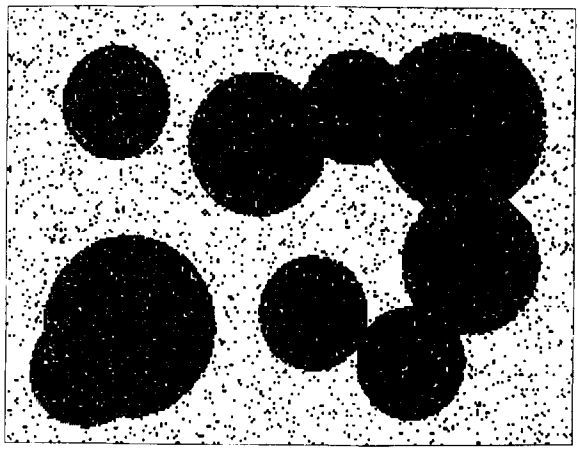

Fig. 11. The output of the image of Fig. 8 with 6 db SNR noise level.

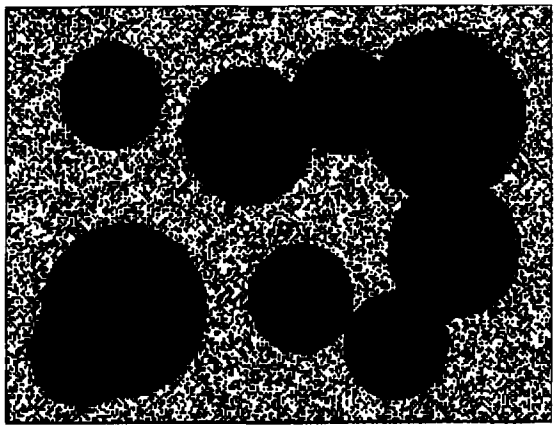

Fig. 10. The output of the image of Fig. 8 with 60% background noise.

successfully detected without using any noise treatment even if the color of 50% background pixels are changed due to noise. See Fig. 10, for example where background noise covers 60%. However, when noise is present both in foreground and background all L_1, L_2 disks could been separated well using the noise removal technique of Section 3.3. See Fig. 11 where the original image SNR is 6 db.

Our algorithm can be implemented in parallel as it is based on morphological operators. Another notable advantage is that computational requirement is fixed and independent of the number of occluded/non-occluded disks in the image.

The proposed algorithm of disk separation can have some real-world applications. It can be used in quality control, inspection and counting of circular objects. For example, in a camera-based system of coin counting, our algorithm can be incorporated.

Detection of gray tone circular discs using gray tone morphological operators is the subject of our future study. Important results on this study will be communicated in near future.

Acknowledgements

One of the authors (A.R. Chaudhuri) wishes to thank the Council of Scientific and Industrial Research (CSIR), India for providing him a research fellowship in pursuing his work.

Appendix A

After estimating all possible existing disk's radii, $r_1, r_2, \ldots, r_N$ identification, location and separation

is performed step by step where the original binary image is E_o.

$E^o \leftarrow E_o$; $E' \leftarrow \phi$; $i \leftarrow 1$;

$E^e \leftarrow E_o \ominus T_{[r_i]}$;

do {

if $(i = N)$ $E^{e(+1)} \leftarrow \phi$;

else $E^{e(+1)} \leftarrow E_o \ominus T_{[r_{i+1}]}$;

$E^{o(+1)} \leftarrow E^{e(+1)} \oplus T_{[r_{i+1}]}$;

$E^{sc} \leftarrow E^e / E^{o(+1)}$;

Perform component labeling on E^{sc} only if $\# E^{sc} > 0$.

[Note that $\# E^{sc} = 0$ indicates that there is no L_1 disk of radius r_i in E_o.]

Suppose jth component is denoted by e_j $(j = 1, 2, \ldots, k)$;
for $j = 1, 2, \ldots, k$

do {

Find the center of mass (CM) of the e_j. Let it be c_j.
[Note that c_j represents the center of the jth (either L_0 or L_1) disk of radius r_i.]

}

$E^{sc} \leftarrow E^{sc} \oplus T_{[r_i]}$;

$E' \leftarrow E' \cup E^{sc}$;

$E^{cre} \leftarrow E^o / E'$;

$E^o \leftarrow E' \leftarrow E^{o(+1)}$;

$E^e \leftarrow E^{e(+1)}$

if $(\# E^{cre} > \pi r_i^2 / 3)$ {

$tf \leftarrow 0.146 \times r_i$;

$E^{cre.e} = E^{cre} \ominus T_{[tf]}$;

Perform component labeling on $E^{cre.e}$.
Suppose jth component is denoted by e_j for $j = 1, 2, \ldots, k'$.
Store it in E^h
for $j = 1, 2, \ldots, k'$
do {

Single-component region growing of e_j in E^{cre}.
Suppose that grown region is stored in E^a.
$E^b \leftarrow E^a / (E^a \ominus T_1)$;
Let m is the maximum s.t. $E^h \ominus mT_{[1]} \neq \phi$;

$E^h \leftarrow E^h \ominus mT_{[1]}$;

$E^{cfr} \leftarrow E^h \oplus |_{E^{o(+1)}} T_{[r_i - tf - m + 1]}$;

$\alpha_c \leftarrow 0$; $\beta_c \leftarrow 0$;

$\forall p(p_x, p_y) \in E^{cfr}$

do {

$\alpha_p = \#(E^a \cap T_{[r_i]}(p_x, p_y))$;

$\beta_p = \#(E^b \cap C_{[r_i]}(p_x, p_y))$;

if $((\alpha_p \geqslant \alpha_c) \wedge (\beta_p \geqslant \beta_c))$

$c \leftarrow p$; $\alpha_c \leftarrow \alpha_p$; $\beta_c \leftarrow \beta_p$;

[Note that c represents the center of an L_2 disk of radius r_i.]

$i \leftarrow i + 1$;

} while $((i \leqslant N) \wedge (\# E^o > 0))$

References

[1] S.N. Biswas and B.B. Chaudhuri, "On the generation of discrete circular objects and their properties", *Computer Vision, Graphics Image Process.*, Vol. CVGIP 32, 1985, pp. 158–170.

[2] P. Chan and W.C. Sin, "New parallel Hough transform for circles", *IEEE Proc. E*, Vol. 138, No. 5, 1991 pp. 335–344.

[3] B.B. Chaudhuri and P. Kundu, "Optimum circular fit to weighted data in multi-dimensional space", *Pattern Recognition Lett.*, Vol. PRL 14, 1993, pp. 1–6.

[4] L.-H. Chen and K.-L. Lee, "A new method for circular object detection and location", *Pattern Recognition Lett.*, Vol. PRL 11, 1990, pp. 691–697.

[5] A. Das and B. Chanda, "Fast algorithm for morphological operations for sequential machines", *Internat. Conf. on Advances in Pattern Recognition and Digital Techniques*, ICAPRDT, Calcutta, India, 28–31 December 1993, pp. 258–266.

[6] E.R. Davies, "A high speed algorithm for circular object location", *Pattern Recognition Lett.*, Vol. PRL 6, 1987, pp. 323–333.

[7] R.M. Haralick, S.R. Sternberg and X. Zhuang, "Image analysis using mathematical morphology", *IEEE Pattern Anal. Machine Intelligence*, Vol. PAMI-9, July 1987, pp. 523–550.

[8] C.-T. Ho and L.-H. Chen, "A high speed method for locating circular objects", *J. Electronic Imaging*, Vol. 2, No. 2, 1993, pp. 100–113.

[9] U.M. Landau, "Estimation of circular arc centre and its radius", *Computer Vision, Graphics and Image Process.*, Vol. CVGIP 38, pp. 317–326.

[10] J.P. Pascual Strarink and I.T. Young, "Localization of circular objects", *Pattern Recognition Lett.*, Vol. PRL14, 1993, pp. 895–905.

[11] D. Schonfeld and J. Goutsias, "Optimal morphological pattern restoration from noisy binary images", *IEEE Pattern Anal. Machine Intelligence*, Vol. PAMI 13, No. 1, 1991, pp. 14–29.

[12] J. Serra, *Image Analysis and Mathematical Morphology*, Academic Press, New York, 1982.

[13] X. Zhou and R. Gordon, "Generation of noise in binary images", *CVGIP: Graphical Models Image Process.*, Vol. 53, No. 5, 1991, pp. 476–478.